Research Article

Growth and Characterizations of Organic NLO Imidazolium L-Tartrate (IMLT) Single Crystal

Hiral Raval [ID]**,[1,2] B. B. Parekh,[1] K. D. Parikh,[3] and M. J. Joshi[4]**

[1]*School of Technology, Pandit Deendayal Petroleum University, Gandhinagar 382007, India*
[2]*L D College of Engineering, Ahmedabad 380015, India*
[3]*M.P. Shah Arts and Science College, Surendranagar 363001, India*
[4]*Department of Physics, Saurashtra University, Rajkot 360005, India*

Correspondence should be addressed to Hiral Raval; hiralshahraval@gmail.com

Good quality single crystals of organic imidazolium L-Tartrate (IMLT) are grown up from aqueous solution by slow solvent evaporation technique. Various structural parameters and monoclinic crystal structure have been confirmed using powder X-ray diffraction method. The presence of various functional groups has been identified by ATR-FTIR. UV-Vis-NIR spectroscopy has shown more than 60% of optical transparency with the lower UV cutoff at 245nm. The optical band gap value of the material is evaluated to be 4.8 eV. Other optical parameters such as refractive index, optical and electrical conductivity, Urbach energy, extinction coefficient, and optical and electrical susceptibility have been evaluated from transmission spectrum data. The above essential parameters manifest appropriate usage of IMLT as an NLO material. The thermogravimetric analysis indicates high thermal stability of material up to 214°C. Apart from that, the dielectric study at various temperatures confirms decrement of dielectric constant and dielectric loss at higher frequencies. The efficiency of Second Harmonic Generation (SHG) is found to be 3.5 times that of the KDP crystals. A range of analysis suggests suitability and potentiality of IMLT crystal for various optoelectronic applications.

1. Introduction

Though the inorganic materials are enjoying their dominance in application of NLO devices, the organic NLO materials are gradually increasing their share in device applications. The organic material crystals with good molecular hyperpolarizability, quadratic nonlinear optical properties, laser damage threshold, molecular nonlinearities, and high structural diversities are preferred for the NLO device applications [1–3]. In recent years, development of various organic donor-π-acceptor (D-π-A) systems has drawn remarkable attention due to their highly polarizable structure and efficient intramolecular charge transfer (CT) properties [4]. Against inorganic material, organic materials have a conveniently polarizable push–pull system which enables their usage for two-photon absorbing contrivance, optoelectronic devices, optical data storage mechanism, and organic LED and photovoltaic cells [5–7].

Imidazole has amphoteric property and high polarizability that is expected to contribute adequately to the optical nonlinearity with other moieties. By adding the conjugated bonds or substituting donors and acceptors, the optical nonlinearity can be increased. In the case of synthesis of the titled compound, the Imidazole donates pair of electrons to L-Tartaric acid. Tartaric acid is a reasonably resilient diprotic chiral α- hydroxyl acid having $pk_{a1}=2.93$ and $pk_{a2}=4.23$. Hence it is potentially adept to form 1:1 and 1:2 proton transfer salts with most of Lewis bases [8], although it is possible to form 1:1 hydrogen tartrate salts using stoichiometric control and large number of them have been studied [9]. The ferroelectricity study of bis(imidazolium) L-Tartrate [10], structural, thermal expansion, laser damage threshold (LDT) and SHG efficiency [11], growth with SR method along with dielectric study [12], and quantum mechanical calculation using DFT [13] of imidazolium L-Tartrate has been reported.
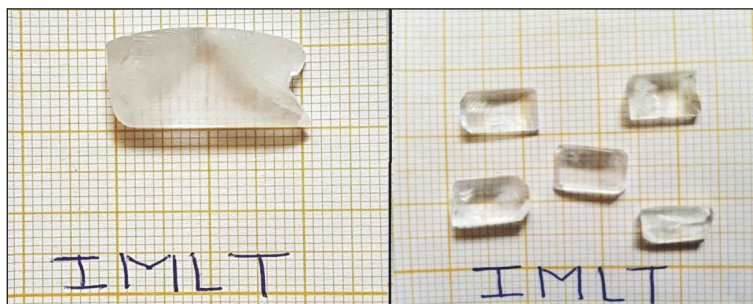
FIGURE 1: IMLT grown crystals with slow evaporation.

In the present work an organic NLO crystal of imidazolium L-Tartrate (IMLT) has been grown and characterized by Powder XRD, FTIR, UV-Vis spectroscopy, Thermogravimetry, and linear optical and SHG studies. Some essential dielectric and optical parameters have been reported furthermore. This collective study with mentioned imperative parameters will facilitate investigating the potential of IMLT single crystal as NLO material and its other applications.

2. Experimental

2.1. Synthesis and Crystal Growth. IMLT has been synthesized through mixing AR mark Imidazole (purity ≥ 99%) and L-Tartaric acid powder (purity ≥ 99.5%) in equimolar ratio (1:1) by dissolving in double distilled water. To obtain a homogeneous solution, mixture was stirred for about 100 min at constant temperature of 40°C using magnetic stirrer. The mixture was filtered with Whatman filter paper no 41 and kept in a glass beaker. The beaker was sealed with perforated polythene cover and kept back at constant temperature of 30°C in a dust free environment. The synthesized solution was purified by successive recrystallization process. After 15 days, transparent, good quality, rectangular crystals were recovered having a maximum size of 20mm x 10mm x 5mm as shown in Figure 1.

2.2. Characterization Techniques. The crystal structure was determined by Powder XRD technique through PANalytical system employing Cu Kα radiation. The results were analyzed with the help of Powder X software. For FTIR study, the material was kept in Bruker Optics Attenuated Total Reflection (ATR) setup in range of 450 cm^{-1} to 4000 cm^{-1}. The UV-Vis-NIR transmission spectrum was recorded for 2.5 mm thick crystalline sample within range of 200 to 1400 nm with a slit width of 5nm and scan speed of 240 nm/min using Perkin Elmer Lambda Spectrophotometer. The scanning range covered near-ultraviolet (200-400 nm), visible (400-800 nm), and NIR (800-1200 nm) regions. Thermal analysis of the material has been carried out from room temperature to 800°C using Perkin Elmer thermal analyzer setup at heating rate of 10°C/minute in N$_2$ atmosphere. The dielectric study was carried from 10 Hz to 10 MHz at different temperatures on pelletized crystals of the known dimensions using PSM-1735 impedance analyzer. The SHG efficiency was evaluated
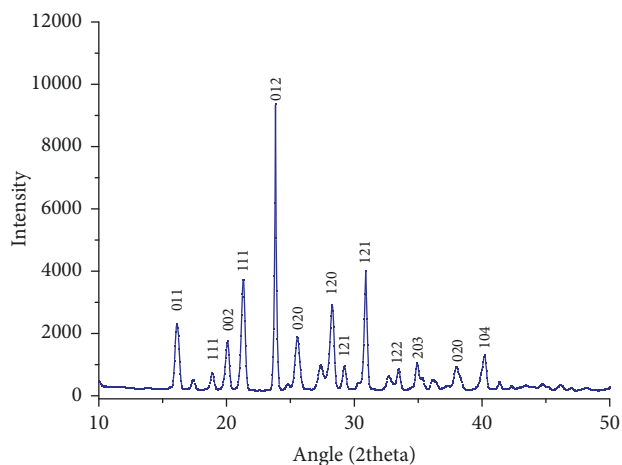

FIGURE 2: Powder XRD pattern of IMLT.

using Kurtz and Perry powder method for Nd:YAG laser of 1064 nm and the result was compared with the standard KDP crystal [14].

3. Results and Discussions

3.1. Powder XRD. The observed diffraction pattern is shown in Figure 2 and cell parameters of IMLT crystals were identified and given in Table 1. The unit cell parameters are found in very good agreement with previously reported values [11, 13]. The crystallite size has been obtained by Scherrer equation, L = Kλ/W cos θ, where k = 0.94, λ = 1.54178 Å, and W is full width at half-maxima. The crystalline size allied with strongest peak (012) is obtained as 59.51nm.

3.2. ATR Spectral Analysis. The subsistence of various functional groups has been recognized using FTIR-ATR spectral response. The observed bands arise due to vibrations of Imidazole cations, tartrate anions, and hydrogen bonds. Figure 3 exhibits FTIR spectrum of IMLT.

The FTIR spectrum of IMLT shows peak referring towards the O-H stretching at 3464.7cm^{-1}. Aromatic stretching due to Imidazole is also observed at 3150.21cm^{-1}. The intensity peak at 1715.7 cm^{-1} of carboxyl group (C=O) band is attributed to L-Tartaric acid. The sharp absorption

TABLE 1: Structural parameters of IMLT.

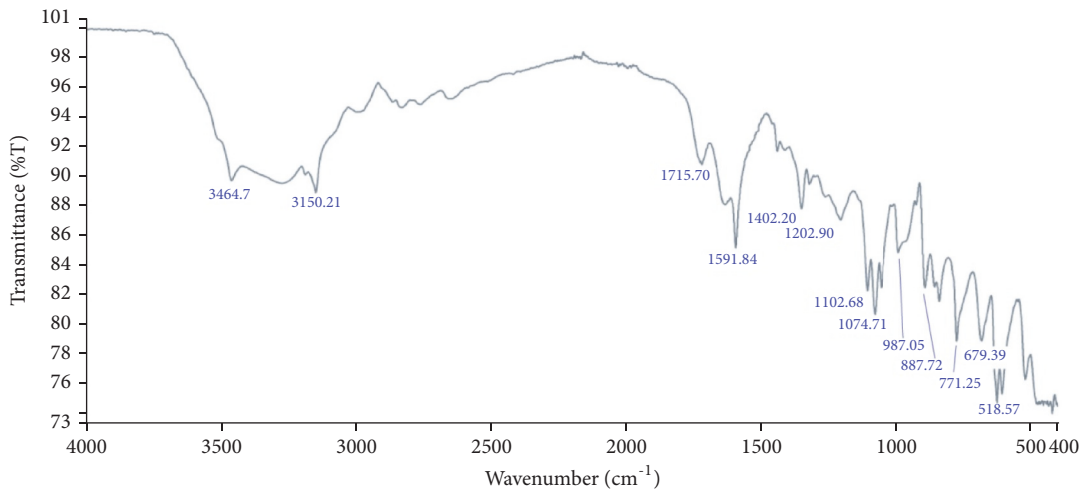| Parameter	Current Study	Reported Value [11]	Reported Value [13]
Crystal Structure	Monoclinic	Monoclinic	Monoclinic
a	7.551 Å	7.587 Å	7.556 Å
b	6.991 Å	6.906 Å	6.961 Å
c	9.034 Å	8.930 Å	9.007 Å
β	101.46°	102.07°	101.457°
Volume (Å)^3	476.896 (Å)^3	455.9 (Å)^3	464.3 (Å)^3

FIGURE 3: FTIR-ATR response of IMLT crystal.

peak at 1591.84 cm^{-1} is observed to be attributed to C=C aromatic ring vibrations. The peaks correspond to C-O bond of carboxylic acid observed at 1202.90 cm^{-1} and 1102.68 cm^{-1}. Absorption peaks at 887.72 cm^{-1}, 771.25 cm^{-1}, and 679.39 cm^{-1} are corresponding to Imidazole aromatic ring.

3.3. UV-Visible Studies. Optical characterization is a vital parameter to be considered for good quality check of crystalline materials. At lower wavelengths, the optical transmission is discontinued in ultraviolet region due to absorption of energy which arises from electronic transition from valance band to unfilled conduction band [15]. Figure 4 displays a plot of %transmittance versus wavelength (nm) of crystal having thickness of 2.5mm. High degree of transparency with no significant absorption is observed within range of 300nm-1400nm. In Figure 4 a strong absorption with a sharp fall of transmittance at 245nm shows lower cutoff wavelength of title compound. This proposes almost homogeneous distribution of energy among all molecules of IMLT crystal, which else will results in a gradual decrease in transmittance from the longer wavelength to 245nm. The undulations witnessed at around 800 nm are due to instrument artefact. Absorption bands observed in the region from 600 nm to 1400 nm are attributed to intramolecular charge transfer transitions among the marginal donor group and acceptor core [16]. Sufficiently low cutoff wavelength and wide transparency window of a crystal suggest good optical quality. The absorption coefficient (α) and the optical parameters, such as
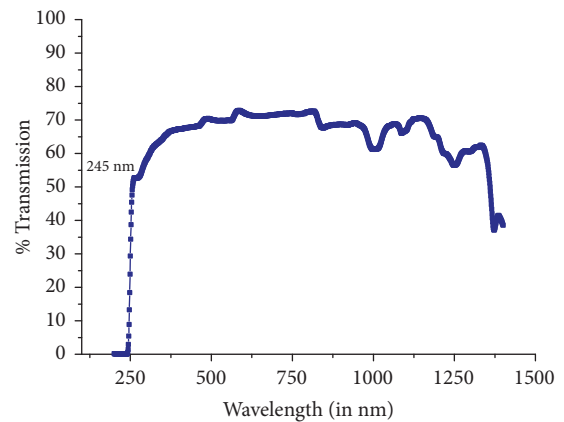

FIGURE 4: UV-Vis-NIR transmission curve of IMLT.

refractive index (η), optical band gap (E$_g$), and extinction coefficient (K), can be determined from the transmission (T) spectrum based on the standard formulas. The crystalline quality has been observed by calculation of Urbach energy value.

The absorption coefficient (α) can be determined by

$$\alpha = \frac{1}{t} \ln \left(\frac{1}{T} \right) \tag{1}$$

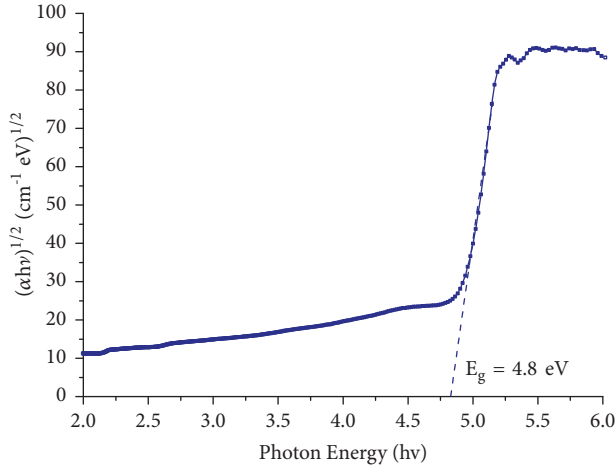where parameter T refers to transmittance and t thickness of crystal.

FIGURE 5: Tauc's plot of IMLT crystal.

FIGURE 6: Change in refractive index with wavelength of IMLT crystal.

The optical band gap (E_g) can be obtained by means of a Planck relation as

$$E_g = h\nu = \frac{hc}{\lambda} \qquad (2)$$

where h is the Planck constant, ν is the wave frequency, and c is the speed of light in vacuum.

Experimentally, it can be estimated by linear extrapolation of an absorption edge and by converting the value of the wavelength (nm) into energy with respect to the same in vacuum (eV). The optical band gap (E_g) is calculated from Tauc's formula [17]

$$\alpha h\nu = B\left(h\nu - E_g\right)^m \qquad (3)$$

where B is a constant, m=2 refers to indirect band-to-band transition, and m=0.5 refers to direct band-to-band transition.

A plot of $(\alpha h\nu)^{1/2}$ versus hν is shown in Figure 5. To decide the optical band gap value experimentally, m=1/2 is found as the best fitted value for the linearity of the plot and that indicates indirect band gap transition. The traversing point on energy axis indicates the band gap energy value of IMLT crystal. The optical band gap value of IMLT crystal is E_g = 4.80 eV. Band gap energy of crystal conveys the capability of dielectric medium (crystal) to be polarized under the effect of strong radiation. The large band gap of IMLT crystal supports the requirement for the good quality nonlinear optical applications.

Refractive index from transmittance value of IMLT crystal can be obtained using the following expression [18, 19].

$$\eta = \frac{1}{T} + \left(\frac{1}{T} - 1\right)^{1/2} \qquad (4)$$

Figure 6 shows change in refractive index with respect to wavelength for IMLT crystal. Refractive index decreases as wavelength increases. The higher band gap, good transmission in overall region, and lower refractive index make the
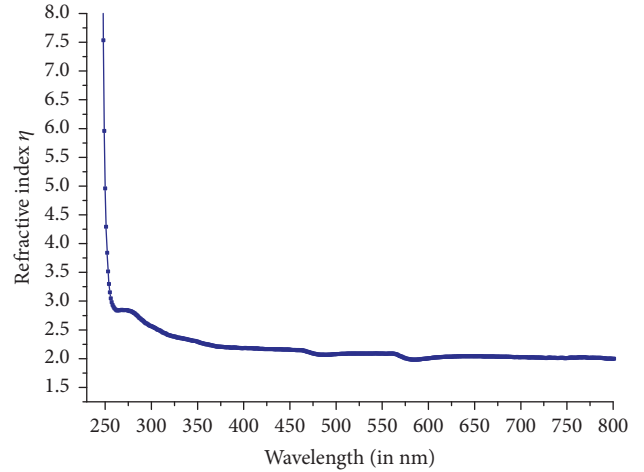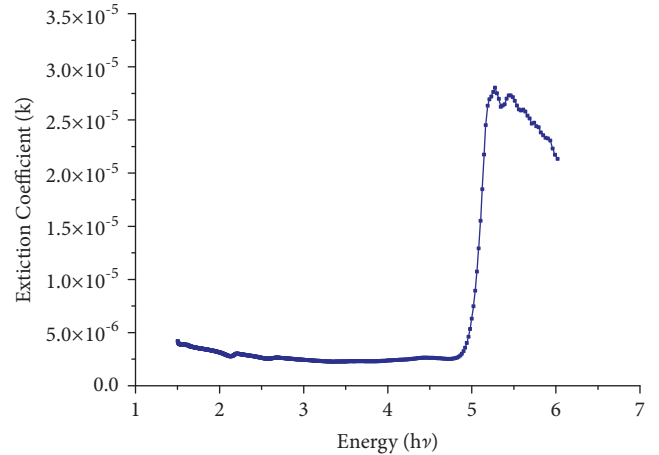

FIGURE 7: Extinction coefficient vs. photon energy curve.

crystal suitable for good optoelectronic applications [20]. The extinction coefficient value specifies loss of electromagnetic radiation via scattering and absorption by crystal per unit thickness. It suggests how easily an electromagnetic wave is passing through the crystal with different photon energy. The extinction coefficient can be calculated from the following expression.

$$K = \frac{\lambda\alpha}{4\pi} \qquad (5)$$

The graph of extinction coefficient and photon energy is given in Figure 7. The lower value of coefficient shows less fractional loss of incident radiation. However, the increased value at higher energy may be attributed to absorption and scattering based upon incident photon energy and nature of scattering centres. The absorption coefficient value exactly below the fundamental edge depends upon photon energy completely, which supports the Urbach relationship [21]. The value of absorption coefficient at band edge for IMLT crystal
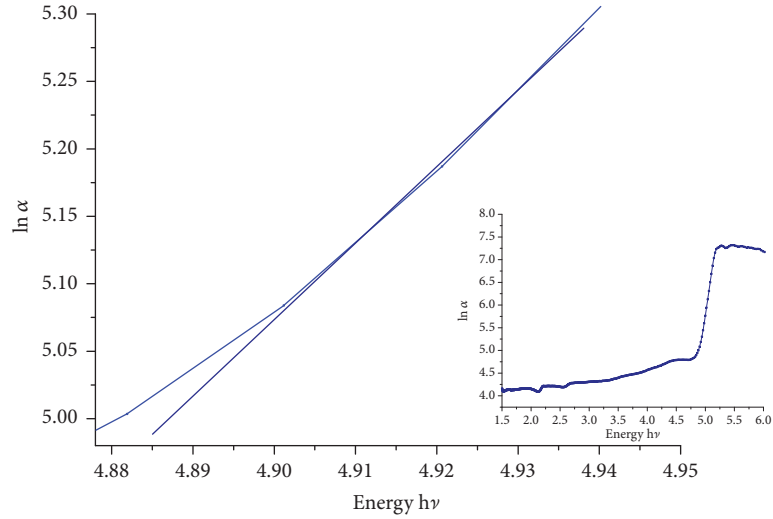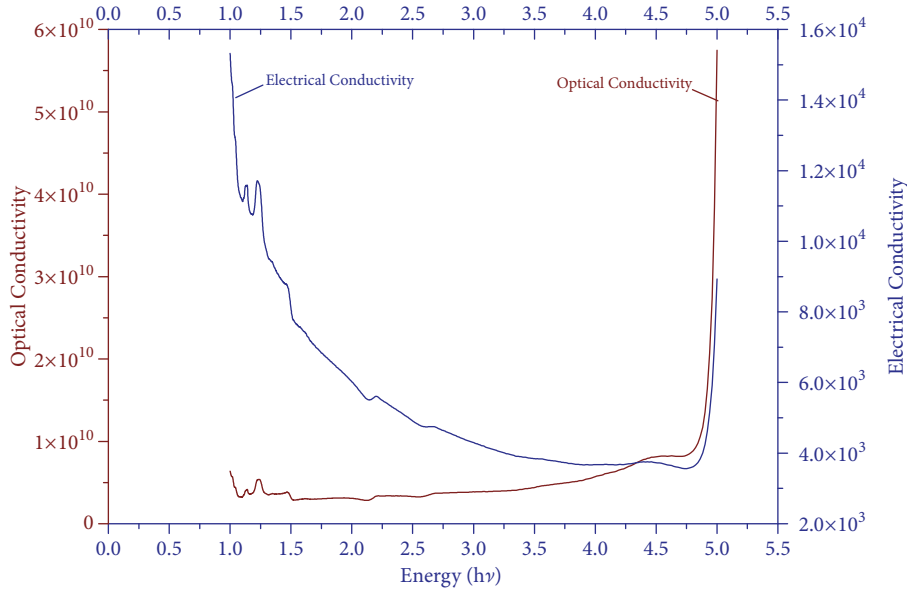
FIGURE 8: Linear portion plot of natural log of the absorption coefficient (α) versus the incident photon energy and its inset.

FIGURE 9: Optical conductivity of IMLT crystal.

manifests exponential dependence on the photon energy ($h\nu$) that gives the Urbach formula

$$\alpha_{h\nu} = \alpha_0 \exp^{(h\nu/E_u)} \qquad (6)$$

where α_0 is a constant, ν is the frequency of incident radiation, and E_u is the value of Urbach energy.

The Urbach energy value was obtained by calculating inverse of the slope observed in linear portion of lower photon energy region as shown in Figure 8. The slope value is found to be 5.1957 and hence the Urbach energy value (E_u) is 0.19 eV. The less value of Urbach energy (E_u) suggests a lesser amount of crystalline defects.

The optical conductivity (σ_{op}) response of IMLT crystal is derived in value of the refractive index and absorption coefficient by the following expression.

$$\sigma_{OP} = \frac{\alpha \eta C}{4\pi} \qquad (7)$$

The value of electrical conductivity of material is also associated with the optical conductivity value of the crystal as follows.

$$\sigma_e = \frac{2\lambda \sigma_{OP}}{\alpha} \qquad (8)$$

The increase in value of optical conductivity with incident photon energy (Figure 9) shows good optical response of the
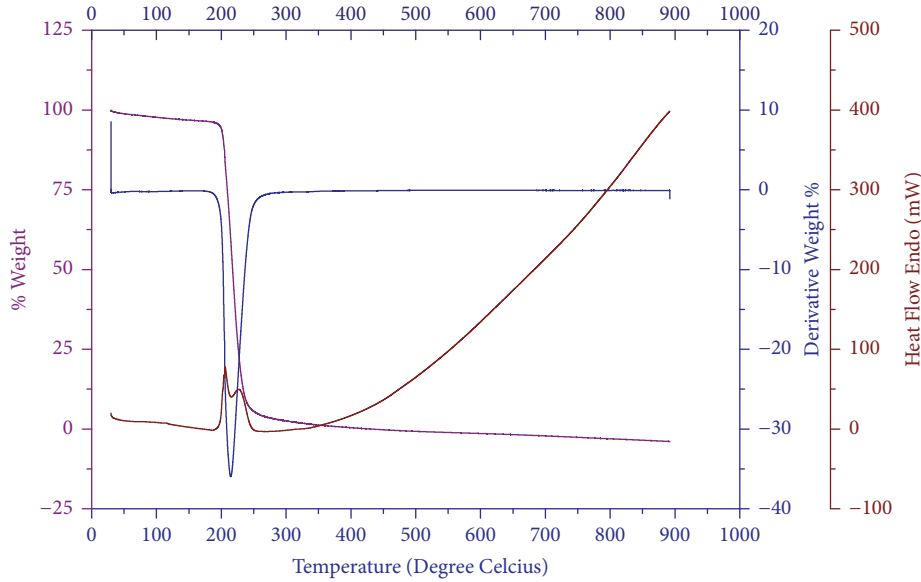
FIGURE 10: Thermal analysis of IMLT crystal.

material. The higher value of optical conductivity (10^9-10^{12} s^{-1}) shows very good photoresponse of IMLT crystals. From graph of extinction coefficient and electrical conductivity, it can be observed that behavior of material is similar to semiconductor at higher energy. Therefore, the material is suitable for optoelectronics device application.

The electric susceptibility (χ_c) can be calculated using optical constant from the following relation [22, 23].

$$\varepsilon_r = \varepsilon_0 + 4\pi\chi_c = \eta^2 - k^2 \tag{9}$$

Therefore

$$\chi_c = \frac{\eta^2 - k^2 - \varepsilon_0}{4\pi} \tag{10}$$

where ε_0 is the dielectric constant in the absence of any contribution from free carriers.

The refractive index calculated from transmission data suggests that it remains constant up to 1100 nm. The value of electrical susceptibility is 0.3848 at 1100 nm (Figure 10). The complex dielectric constant is given by ε_c. The real and imaginary part of dielectric constant from extinction coefficient are given as [23–25]

$$\varepsilon_c = \varepsilon_r + \varepsilon_i \tag{11a}$$

$$\varepsilon_r = n^2 - k^2 \tag{11b}$$

$$\varepsilon_i = 2nk \tag{11c}$$

where ε_r and ε_i are real and imaginary part of dielectric constant, respectively.

At 1100 nm wavelength the values of real ε_r and imaginary ε_i of dielectric constant are 4.8331 and 2.92×10^{-5}, respectively.

3.4. Thermal Analysis. The thermal analysis provides information regarding phase transition, existence of water of crystallization, and different stages of decomposition of the crystal [26]. The IMLT sample of 20.8 mg was analyzed from 25-800°C range in N$_2$ atmosphere (Figure 10). TGA analysis of material revealed that the crystal is stable up to 214.6°C. The weight loss of material is found in single decomposition step in the range of 205°C to 250°C with 88.66% of total weight. The small trace of endothermic peak at 200°C indicates melting followed by decomposition around 220°C. The sharp DTA peak shows good degree of crystallinity and purity of material. The thermal analysis suggests good thermal stability of title compound for any optoelectronic applications below 200°C.

3.5. Dielectric Analysis. The SHG is proportional to linear susceptibility, and the linear susceptibility depends on polarizability; further, the dielectric constant in frequency range should be studied [27]. Therefore, it is important to study the dielectric behavior with frequency of applied field at different temperatures. Figures 11(a) and 11(b) show the dielectric constant (ε_r) and dielectric loss (tan δ) with frequency, respectively. From the graphs, it is found that the same decreases with increases in frequency. The higher value of dielectric constant at low frequencies may be attributed to the existence of all of the four polarization mechanisms, namely, electronic (within atoms), ionic (between molecules), interfacial, and orientational polarization, and its lower value at higher frequency may suggest the loss of implication of these polarization mechanisms gradually. The dielectric loss at 30°C temperature and lower frequencies is little high (Figure 11(b)) maybe due to contribution of electronic polarization, as frequency increases contribution of other polarization mechanisms which are prominent with increase in frequency and temperature. Almost similar behavior is observed from 10 KHz in all other ranges of temperature. The lower value of dielectric loss at higher frequencies at different
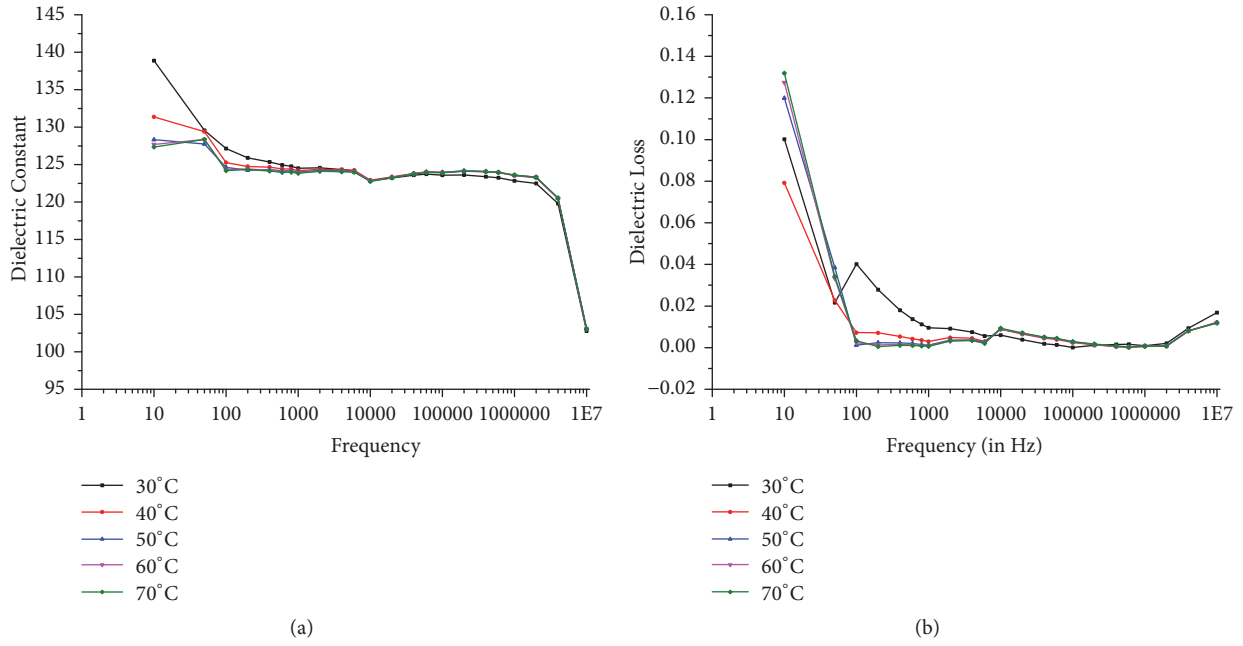
FIGURE 11: (a) Dielectric constant vs. frequency. (b) Dielectric loss vs. frequency measured at different temperatures.
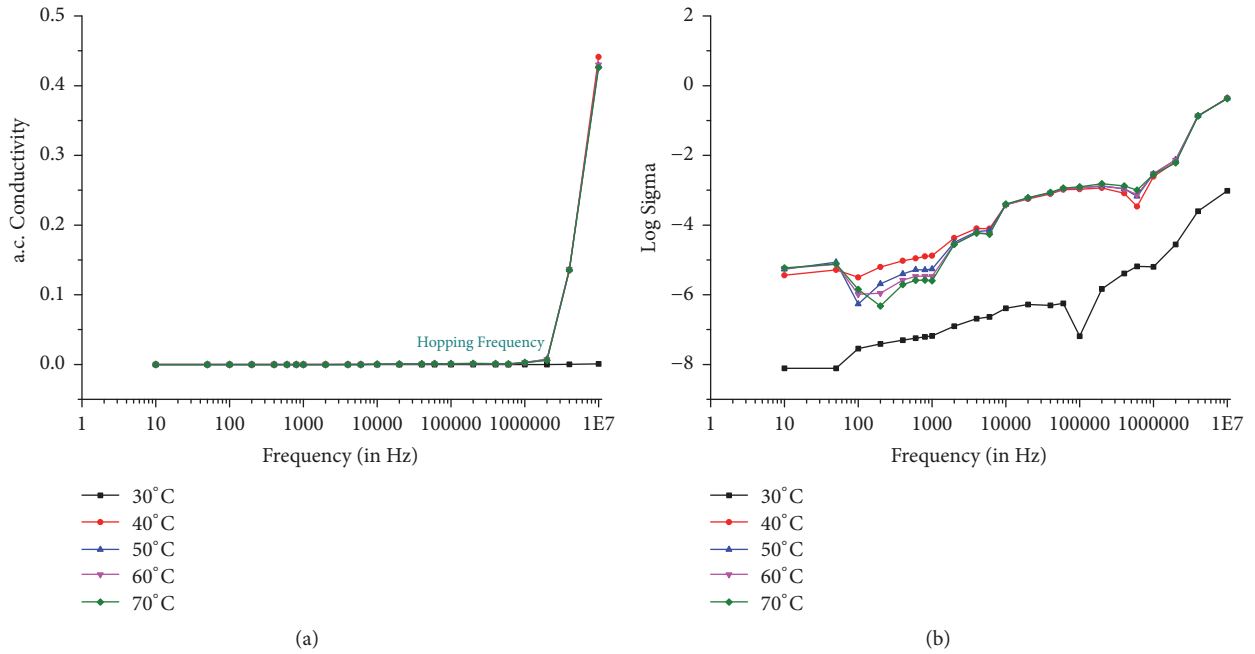

FIGURE 12: (a) AC conductivity versus frequency. (b) Jonscher's plot of log sigma versus frequency.

temperature divulges the good optical quality of the crystal with fewer defects, which is the desirable property for NLO applications [28].

Frequency dependence of conductivity in a material can be investigated from Jonscher's power law [29] and is plotted in Figures 12(a) and 12(b).

$$\sigma_T(\omega) = \sigma_0 + A\omega^s \qquad (12)$$

Here $\sigma_T(\omega)$ is the sum of dc and ac conductivity of material. The term $\sigma_{(0)}$ in equation is the frequency independent d.c. conductivity of material. The second term of right hand side equation represents ac conductivity consisting of coefficient "A" which indicates the strength of polarizability and exponent "s" which represents degree of correlation of lattice with mobile ions. Table 2 indicates the values of "A" and "s" which are temperature dependent and characterize all dispersion phenomena. Generally values of "s" can vary differently from

TABLE 2: Jonscher's law parameters with temperature.

Temperature ($^{\circ}$C)	A ($S\ m^{-1} rad^{-n}$)	S
30	8.43646 x10^{-10}	0.93224
40	1.96309 x 10^{-09}	0.80073
50	4.67563 x 10^{-08}	0.83174
60	3.12306 x 10^{-08}	0.82525
70	6.22558 x 10^{-07}	0.83315

TABLE 3: Nonlinear observation of IMLT and its comparison with KDP.

Sample Name	Input Energy (millijoule)	Output Energy (joule)
KDP	0.70	31.3
IMLT	0.70	8.94

material to material depending on temperature within a range of 0 to 1. For value of s ≤ 1 sudden hopping motion is observed which is attributed to translational motion. For ionic conductors, value of "s" lies between 0.5 and 1. The frequency independent plateau-like region observed in the low frequency regime can be attributed to the frequency independent conductivity $\sigma_{(0)}$. From Figure 12(a), the conductivity increases significantly at higher frequency. At room temperature, behavior is almost unchanged in entire region. This may be due to role of polarization at lower temperature.

3.6. NLO Study. The Second Harmonic Generation (SHG) efficiency of fundamental laser pulse has been assessed using the Kurtz and Perry powder method [14]. A Q-switched beam of Nd:YAG laser, having wavelength of 1064 nm with input beam energy of 0.70 joule and pulse width of 6 ns with repetition rate of 10 Hz, was used. Powder sample of grown IMLT crystal was packed and exposed to laser radiation. A green light flash emission was observed, which indicates NLO behavior of the material. From Table 3 it can be seen that IMLT has a Second Harmonic Generation (SHG) conversion efficiency of 3.5 times that of the standard KDP crystals. The zigzag chain structure of the title compound supports higher SHG. The Π- electron system of the Imidazole ring improves the SHG efficiency of the IMLT crystal associated with L-Tartaric acid, whose NLO conversion efficiency is remarkable with the KDP.

4. Conclusion

Single crystals of IMLT were successfully grown by slow evaporation solution growth technique at constant temperature of 30°C. The X-ray diffraction analysis confirmed monoclinic crystal structure and lattice parameters. Existence of functional groups is confirmed using FTIR-ATR analyses. UV spectral analysis revealed lower UV cutoff at 245nm with wide transparency window. Calculation of optical band gap (E_g), refractive index, absorption coefficient, extinction coefficient, optical and electrical conductivity, and

real and imaginary values of dielectric constants from UV spectrum proposes suitability of material for optoelectronic application. TG/DTA suggests thermal stability of material up to 200°C. Dielectric measurements were carried out using dielectric constant and loss at different frequencies and temperature. The ac conductivity variation with frequency obeys the Jonscher's power law. The 3.5-time greater efficiency of second order NLO and then that of the standard KDP crystal make it promising NLO material.

Data Availability

The XRD, FTIR, UV-Visible, and dielectric data used to support the findings of this study are available from the corresponding author upon request.

Disclosure

Conflicts of Interest

The authors declare that there are no conflicts of interest regarding the publication of this paper.

Acknowledgments

References

[1] R. Silbey, "Chapter I-1 - The structure and properties of the organic solid state," in *Nonlinear Optical Properties of Organic Molecules and Crystals*, D. S. Chemla and J. Zyss, Eds., vol. 1, pp. 3–20, 1987.

[2] H. S. Nalwa and S. Miyata, *Nonlinear Optics of Organic Molecules and Polymers*, CRC Press, Boca Raton, FL, USA, 1997.

[3] S. Basu, "A review of nonlinear optical organic materials," *Industrial & Engineering Chemistry Product Research and Development*, vol. 23, pp. 183–186, 1984.

[4] F. Bureš, O. Pytela, T. Mikysek, and J. Ludvík, "Imidazole as a donor/acceptor unit in charge-transfer chromophores with extended π-linkers," *Chemistry - An Asian Journal*, vol. 6, no. 6, pp. 1604–1612, 2011.

[5] S. R. Forrest and M. E. Thompson, "Introduction: organic electronics and optoelectronics," *Chemical Reviews*, vol. 107, pp. 923–1386, 2007.

[6] G. S. He, L. S. Tan, Q. Zheng, and P. N. Prasad, "Multiphoton absorbing materials: molecular designs, characterizations, and applications," *Chemical Reviews*, vol. 108, pp. 1245–1330, 2008.

[7] Y. Ohmori, "Development of organic light-emitting diodes for electro-optical integrated devices," *Laser & Photonics Reviews*, vol. 4, pp. 300–310, 2009.

[8] G. Smith, D. Wermutha, and J. M. White, "Hydrogen bonding in proton-transfer compounds of 5-sulfosalicylic acid with bicyclic heteroaromatic Lewis bases," *Acta Crystallographica*, vol. C60, pp. o575–o581, 2004.

[9] G. Smith, D. Wermutha, and J. M. Whiteb, "One-dimensional hydrogen-bonded structures in the 1:1 proton-transfer compounds of 4,5-dichlorophthalic acid with 8-hydroxyquinoline, 8-aminoquinoline and quinoline-2-carboxylic acid (quinaldic acid)," *Acta Crystallographica*, vol. C62, pp. o694–o698, 2006.

[10] M. Szafranski, "Comment on ferroelectricity in bis(imidazolium) l-tartrate," *Angewandte Chemie International Edition in English*, vol. 52, p. 7076, 2013.

[11] C. Ji, T. Chen, Z. Sun et al., "Bulk crystal growth and characterization of imidazolium L-tartrate (IMLT): a novel organic nonlinear optical material with a high laser-induced damage threshold," *CrystEngComm*, vol. 15, p. 2157, 2017.

[12] V. Thayanithi and P. Praveen Kumar, "Growth and characterization of unidirectional grown imidazolium L-tartrate (IMLT) single crystal by SR method," *Mechanics, Materials Science & Engineering*, vol. 9, p. 98, 2017.

[13] K. Meena, K. Muthu, V. Meenatchi, M. Rajasekar, G. Bhagavannarayana, and S. P. Meenakshisundaram, "Growth, crystalline perfection, spectral, thermal and theoretical studies on imidazolium l-tartrate crystals," *Spectrochimica Acta Part A: Molecular and Biomolecular Spectroscopy*, vol. 124, p. 663, 2014.

[14] S. K. Kurtz and T. T. Perry, "A powder technique for the evaluation of nonlinear optical materials," *Journal of Applied Physics*, vol. 39, no. 8, pp. 3798–3813, 1968.

[15] Y. Kinger, Bowen, and Uhlmann, *Text Book Introduction to Ceramics, Optical Properties, Chapter 13*, 1976.

[16] N. Vijayan, R. Ramesh Babu, R. Gopalakrishnan, P. Ramasamy, and W. T. A. Harrison, "Growth and characterization of benzimidazole single crystals: a nonlinear optical material," *Journal of Crystal Growth*, vol. 262, pp. 490–498, 2004.

[17] G. Qian, B. Dai, M. Luo et al., "Band gap tunable, donor–acceptor–donor charge-transfer heteroquinoid-based chromophores: near infrared photoluminescence and electroluminescence," *Chemistry of Materials*, vol. 20, pp. 6208–6216, 2008.

[18] J. Tauc, A. Menth, and D. L. Wood, "Optical and Magnetic Investigations of the Localized States in Semiconducting Glasses," *Physical Review Letters*, vol. 25, no. 11, pp. 749–752, 1970.

[19] N. A. Bakr, A. M. Funde, V. S. Waman et al., "Determination of the optical parameters of a-Si:H thin films deposited by hot wire-chemical vapour deposition technique using transmission spectrum only," *Pramana—Journal of Physics*, vol. 76, no. 3, pp. 519–531, 2011.

[20] J. H. Joshi, S. Kalainathan, D. K. Kanchan, M. J. Joshi, K. D. Parikh, and J. Arabian, "Effect of l-threonine on growth and properties of ammonium dihydrogen phosphate crystal," *Arabian Journal of Chemistry*, 2017.

[21] P. Rajesh and P. Ramasamy, "Growth of dl-malic acid-doped ammonium dihydrogen phosphate crystal and its characterization," *Journal of Crystal Growth*, vol. 311, pp. 3491–3497, 2009.

[22] F. Urbach, "The long-wavelength edge of photographic sensitivity and of the electronic absorption of solids," *Physical Review A: Atomic, Molecular and Optical Physics*, vol. 92, no. 5, pp. 1324-1325, 1953.

[23] V. Gupta and A. Mansingh, "Influence of postdeposition annealing on the structural and optical properties of sputtered zinc oxide film," *Journal of Applied Physics*, vol. 80, no. 2, pp. 1063–1073, 1996.

[24] A. P. Kochuparampil, J. H. Joshi, and M. J. Joshi, "Growth, structural, spectroscopic, thermal, dielectric and optical study of cobalt sulphide-doped ADP crystals," *Modern Physics Letters B*, vol. 27, Article ID 1750246, 2017.

[25] P. Dhanaraj, T. Suthan, and N. Rajesh, "Synthesis, crystal growth and characterization of a semiorganic material: Calcium dibromide bis(glycine) tetrahydrate," *Current Applied Physics*, vol. 10, no. 5, pp. 1349–1353, 2010.

[26] M. A. Gaffar, A. Abu El-Fadl, and S. Bin Anooz, "Influence of strontium doping on the indirect band gap and optical constants of ammonium zinc chloride crystals," *Physica B: Condensed Matter*, vol. 327, pp. 43–54, 2003.

[27] F. Q. Meng, M. K. Lu, Z. H. Yang, and H. Zeng, "Thermal and crystallographic properties of a new NLO material, urea-(d) tartaric acid single crystal," *Materials Letters*, vol. 33, no. 5-6, pp. 265–268, 1998.

[28] R. C. Miller, "Optical second harmonic generation in piezoelectric crystals," *Applied Physics Letters*, vol. 5, pp. 17–19, 1964.

[29] J. H. Joshi, D. K. Kanchan, M. J. Joshi, H. O. Jethva, and K. D. Parikh, "Dielectric relaxation, complex impedance and modulus spectroscopic studies of mix phase rod like cobalt sulfide nanoparticles," *Materials Research Bulletin*, vol. 93, pp. 63–73, 2017.